Port-Hamiltonian model of a flexible manipulator test rig

Mei Wang[1]
Technical University of Munich, Department of Mechanical Engineering,
Chair of Automatic Control, Boltzmannstraße 15, 85748 Garching, Germany
E-Mail: mei.wang@tum.de

Paul Kotyczka[2]
Univ Lyon, Université Claude Bernard Lyon 1, CNRS, LAGEP UMR 5007,
43 Boulevard du 11 Novembre 1918, 69622 Villeurbanne Cedex, France
E-mail: kotyczka@tum.de

Abstract

We present the modeling of a single-link flexible manipulator test rig, which consists of lumped and distributed parameter subsystems, in the port-Hamiltonian (PH) framework. We focus on discretization issues for the flexible structure and the interconnection of the subsystems to obtain the complete PH model. The flexible structure is modeled as a Timoshenko beam, and the finite-dimensional model is obtained by a geometric pseudo-spectral discretization that preserves the PH structure. The overall manipulator model serves as a basis for feedforward and feedback control design, where structural properties of the PH formulation are exploited to achieve highly dynamic motion control on the test rig.

1 Introduction

Light-weight manipulators have been developed in order to realize highly dynamic motion at a large payload-to-mass ratio and with low energy consumption compared to conventional heavy rigid robot, see e. g. [11]. The structural and joint elasticity requires to treat them as flexible multi-body mechanical systems, which increases the complexity for modeling, motion planning and control [5]. As pointed out in [13], the port-Hamiltonian (PH) approach represents a quite natural perspective to tackle problems in multi-body flexible systems: All components (e. g. rigid bodies, flexible links and kinematic pairs) are modeled separately as PH subsystems. Their coupling via power-preserving interconnections produces an overall system model, in which the PH structure is preserved. The existence of structural invariants (so-called Casimir functionals) is the basis for output feedback control of flexible structures in the PH framework, see e.g. [16]. To obtain finite-dimensional PH models of distributed parameter subsystems, a structure-preserving discretization, see e.g. [6], [15] must be performed. The resulting discrete models can also be exploited for feedback control [12]. See [2] for a general overview of the PH approach to modeling and control of multiphysics systems.
In this contribution, we consider the modeling of a single-link flexible manipulator which is the first stage of a modular test rig, currently set up at the Chair of Automatic Control. An elastic steel beam is fixed on a rigid hub and driven by a gear motor in the horizontal plane. The gear

[1]Mei Wang gratefully acknowledges the financial support from Deutsche Forschungsgemeinschaft (DFG), project KO 4750/1-1

[2]Paul Kotyczka is on temporary leave from Technical University of Munich, Chair of Automatic Control, with financial support by European Union's Horizon 2020 research and innovation programme (Marie Skłodowska-Curie Individual Fellowship, grant agreement No 655204, EasyEBC) and the DFG-ANR project INFIDHEM, project ID ANR-16-CE92-0028.

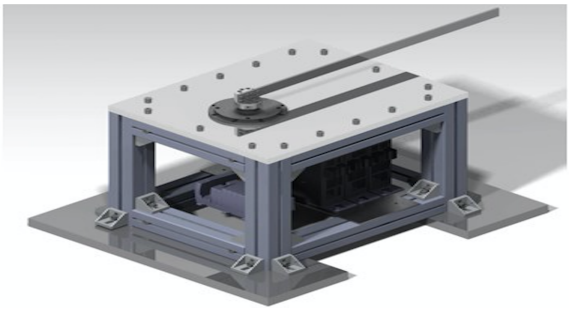

Figure 1: Flexible link test rig.

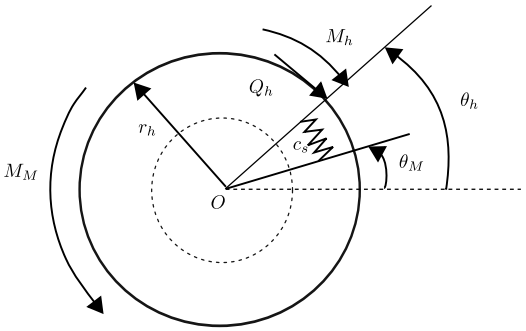

Figure 2: Sketch of a gear motor, cf. [4].

motor and rotating Timoshenko beam are described separately in PH form. A geometric spatial discretization of the beam model is performed with the pseudo-spectral approach presented in [15]. The PH structure is exploited to couple both finite-dimensional subsystem models by interconnection.
The contribution is organized as followed: Section 2 presents the PH models of the gear motor and the Timoshenko beam. A structure-preserving spatial discretization is performed for the latter, before the models are interconnected. Section 3 contains a discussion on the choice of collocation points for the pseudo-spectral discretization of the beam and the assessment of the approximation quality in terms of the spectrum, eigenfunctions and frequency response. Conclusion and an outlook to future work are given in Section 4.

2 Modeling

Figure 1 depicts the lab setup for the single-link flexible manipulator. The beam, which is connected to the gear motor via a hub, exerts a planar motion. The core task for modeling and control of the light-weight manipulator is to deal with the vibration of the flexible structure, which is described by partial differential equations. Timoshenko theory provides an accurate description of the dynamics by taking into account the shear forces and rotatory inertia. The Timoshenko beam is a popular example for modeling and control based on the port-Hamiltonian (PH) representation of distributed parameter systems, while the gear motor system can be easily described by ordinary differential equations.

2.1 Gear motor

The drive system of the manipulator consists of a brushless DC electric motor (BLDC motor) with a Harmonic Drive® gear and a rigid hub. The gear elasticity can be approximated by a linear torsion spring (see e. g. [4]). Instead of directly connecting on the gear box, the beam is fixed on a rigid hub whose mass and moment of inertia shouldn't be neglected.

Equations of motion. Figure 2 shows a sketch of the gear motor, similar to [4], page 58. According to the Newton's second law, the equations of motion can be described by two degrees of freedom at the driven side:

$$I_M \ddot{\theta}_M = M_M - c_s(\theta_M - \theta_h) \tag{1}$$

$$I_h \ddot{\theta}_h = c_s(\theta_M - \theta_h) - M_h - Q_h r_h. \tag{2}$$

The indices m and M refer to quantities on the driving and driven side, respectively.

$$I_M = n^2 I_m, \quad M_M = n M_m, \quad \theta_M = \frac{\theta_m}{n}, \tag{3}$$

are the motor moment of inertia[3], the motor torque and the rotation angle at the *driven* side for a gear ratio $n > 1$. The motor output torque M_M will be considered the system input. θ_h indicates the hub angle, which is in general $\theta_h \neq \theta_M$. The linear spring force $M_s = c_s(\theta_M - \theta_h)$ represents the gear elasticity. M_h and Q_h are the bending torque and shear force due to the beam reaction.

Port-Hamiltonian representation. We define the the state vector

$$\boldsymbol{x}_a(t) = \begin{bmatrix} \theta_M & \theta_h & p_M & p_h \end{bmatrix}^T, \tag{4}$$

which is composed of the drive angles θ_M and θ_h as well as the angular momenta $p_M = I_M \dot{\theta}_M$ and $p_h = I_h \dot{\theta}_h$. The energy of the drive system consists of the kinetic and elastic potential part:

$$H_a = \frac{1}{2}\left(\frac{p_M^2}{I_M} + \frac{p_h^2}{I_h} + c_s(\theta_M - \theta_h)^2\right). \tag{5}$$

The *co-energy* variables are defined by the gradient of the Hamiltonian,

$$\left(\frac{\partial H_a}{\partial \boldsymbol{x}_a}\right)^T = \begin{bmatrix} c_s(\theta_M - \theta_h) \\ -c_s(\theta_M - \theta_h) \\ \dot{\theta}_M \\ \dot{\theta}_h \end{bmatrix}, \tag{6}$$

and represent the spring forces, the motor driven and the hub angular speed, respectively. The equations of motion (1) can now be rewritten in port-Hamiltonian form as

$$\begin{aligned} \dot{\boldsymbol{x}}_a &= \boldsymbol{J}_a \left(\frac{\partial H_a}{\partial \boldsymbol{x}_a}\right)^T + \boldsymbol{B}_a \boldsymbol{u}_a \\ \boldsymbol{y}_a &= \boldsymbol{B}_a^T \left(\frac{\partial H_a}{\partial \boldsymbol{x}_a}\right)^T \end{aligned} \tag{7}$$

with the interconnection and input matrix

$$\boldsymbol{J}_a = \begin{bmatrix} \boldsymbol{0}_{2\times 2} & \boldsymbol{I}_2 \\ -\boldsymbol{I}_2 & \boldsymbol{0}_{2\times 2} \end{bmatrix}, \qquad \boldsymbol{B}_a = \begin{bmatrix} 0 & 0 & 1 & 1 \\ 0 & 0 & 0 & r_h \\ 0 & 0 & 0 & 1 \end{bmatrix}^T.$$

The vectors $\boldsymbol{u}_a, \boldsymbol{y}_a \in \mathbb{R}^3$ of inputs and collocated, power-conjugated outputs are

$$\boldsymbol{u}_a = \begin{bmatrix} M_M \\ \hdashline -Q_h \\ -M_h \end{bmatrix} = \begin{bmatrix} u_{a_1} \\ \boldsymbol{u}_{a_2} \end{bmatrix}, \qquad \boldsymbol{y}_a = \begin{bmatrix} \dot{\theta}_M \\ \hdashline v_h \\ \dot{\theta}_h \end{bmatrix} = \begin{bmatrix} y_{a_1} \\ \boldsymbol{y}_{a_2} \end{bmatrix}, \tag{8}$$

where $v_h = \frac{\dot{\theta}_h}{r_h}$ denotes the translational velocity of the hub and $\boldsymbol{u}_{a_2}$ contains the reaction force and torque of the beam.

[3] I_m consists of the moment of inertia of the rotor and fast rotating gear part.

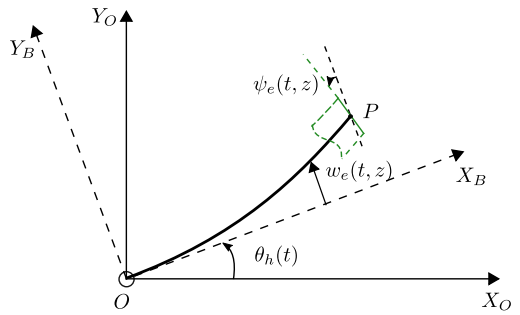

Figure 3: Beam with coordinate systems [3]

Parameter	Value	Unit
Length	0.65	m
Width	0.03	m
Depth	0.005	m
Volumetric mass density	7850	$\mathrm{kg\,m^{-3}}$
Young's modulus	210	GPa
Poisson's ratio	0.34	–
Shear correction factor	$\frac{5}{6}$	–

Table 1: Parameters of a steel beam

2.2 Timoshenko beam

We introduce the model of the Timoshenko beam in PH form and summarize its structure-preserving discretization that leads to a finite-dimensional PH state space model as in [19].

2.2.1 Distributed parameter model

Figure 3 depicts the total motion of Timoshenko beam which consists of a rigid rotation $\theta_h(t)$, the flexible displacement from the equilibrium position $w_e(t,z)$ and the rotation of the beam's cross section due to bending $\psi_e(t,z)$ at a point z along the beam length[4]. The shear angle $\gamma = \partial_z w_e(t,z) - \psi_e(t,z)$ is non-zero according to the Timoshenko theory. Additionally, we assume that the beam length doesn't change during the movement.

Classical beam equations. In many engineering applications, as well as in our case, only small deformations with respect to a reference configuration occur, so that the linearized model can be used, see e. g. [3]. The two linear second order PDEs on $\mathbb{R}^+ \times [0, L]$ are considered

$$\begin{aligned} \rho\partial_t^2 w - K_s(\partial_z^2 w - \partial_z\psi) &= 0 \\ I_\rho\partial_t^2\psi - K_b\partial_z^2\psi + K_s(\psi - \partial_z w) &= 0, \end{aligned} \tag{9}$$

describe the total deflection $w(t,z)$ and rotation $\psi(t,z)$ of the beam's cross section

$$w(t,z) = w_e(t,z) + z\theta_h(t), \qquad \psi(t,z) = \psi_e(t,z) + \theta_h(t). \tag{10}$$

The physical parameters ρ, I_ρ, K_s and K_b are respectively the line density, mass moment of inertia of cross section, shear and flexural stiffness. In most references, the latter are defined by $K_s = \kappa GA$ and $K_b = EI$, where the shear correction factor κ depends on the shape of the cross section. A is the cross sectional area, G is the shear modulus, E is Young's Modulus and I is the area moment of inertia. For $\theta_h(t) = 0$, Eqs. (9) describe the quasistatic Timoshenko beam model (see [10]).

Port-Hamiltonian formulation. According to [9], we define a vector of distributed state variables $\boldsymbol{x}_b(t,z) \in \mathbb{R}^4$ as

$$\boldsymbol{x}_b = \begin{bmatrix} p_t & p_r & \epsilon_t & \epsilon_r \end{bmatrix}^T = \begin{bmatrix} \rho\partial_t w & I_\rho\partial_t\psi & \partial_z w - \psi & \partial_z\psi \end{bmatrix}^T \tag{11}$$

[4]We consider only a planar motion of beam in the rectangular coordinate system, so that we define a generalized coordinate z as the spatial coordinate along the beam to describe the 1D deformation.

with $p_t(t,z)$, $p_r(t,z)$ the translational and angular momentum densities, and $\epsilon_t(t,z)$, $\epsilon_r(t,z)$ the shear and rotational strains. The total Hamiltonian is $H_b = \int_0^L \mathcal{H}_b dz$ with energy density

$$\mathcal{H}_b = \frac{1}{2\rho} p_t^2 + \frac{1}{2I_\rho} p_r^2 + \frac{1}{2} K_s \epsilon_t^2 + \frac{1}{2} K_b \epsilon_r^2. \tag{12}$$

Due to the horizontal configuration of the manipulator, no gravitational energy terms occur. The vector of (distributed) effort variables $\boldsymbol{e}_b(t,z)$ can be expressed as $\boldsymbol{e}_b = (\partial_{\boldsymbol{x}_b} \mathcal{H}_b)^T = (\delta_{\boldsymbol{x}_b} H_b)^T$, where $\delta_{\boldsymbol{x}_b} H_b$ denotes the (row) vector of variational derivatives of the energy functional:

$$\boldsymbol{e}_b(t,z) = \begin{bmatrix} e^{p_t} \\ e^{p_r} \\ e^{\epsilon_t} \\ e^{\epsilon_r} \end{bmatrix} = \begin{bmatrix} \delta_{p_t} H_b \\ \delta_{p_r} H_b \\ \delta_{\epsilon_t} H_b \\ \delta_{\epsilon_r} H_b \end{bmatrix} = \begin{bmatrix} p_t/\rho \\ p_r/I_\rho \\ K_s \epsilon_t \\ K_b \epsilon_r \end{bmatrix}. \tag{13}$$

The effort or co-state variables represent translational and angular velocity as well as shear force and bending moment. The two second order PDEs (9) can be rewritten as a system of forth order equations:

$$\dot{\boldsymbol{x}}_b = (\boldsymbol{P}_1 \partial_z + \boldsymbol{P}_0)(\delta_{\boldsymbol{x}_b} H_b)^T, \qquad \boldsymbol{P}_1 = \begin{bmatrix} 0 & 0 & 1 & 0 \\ 0 & 0 & 0 & 1 \\ 1 & 0 & 0 & 0 \\ 0 & 1 & 0 & 0 \end{bmatrix}, \; \boldsymbol{P}_0 = \begin{bmatrix} 0 & 0 & 0 & 0 \\ 0 & 0 & 1 & 0 \\ 0 & -1 & 0 & 0 \\ 0 & 0 & 0 & 0 \end{bmatrix}. \tag{14}$$

$\boldsymbol{P}_1 \partial_z + \boldsymbol{P}_0$ is a formally skew-adjoint differential operator, see e. g. [9]. Defining the vector of flows $\boldsymbol{f}_b(t,z) = -\dot{\boldsymbol{x}}_b$, the time derivative of H_b can be written as

$$\dot{H}_b = \int_0^L \delta_{\boldsymbol{x}_b} H_b \, \dot{\boldsymbol{x}}_b \, dz = -\int_0^L \boldsymbol{e}_b^T(z) \boldsymbol{f}_b(z) \, dz. \tag{15}$$

Replacing the right hand side of (14) for the flows and applying integration by parts, we obtain

$$\dot{H}_b = \left(e^{p_t} e^{\epsilon_t} + e^{p_r} e^{\epsilon_r} \right) \Big|_0^L, \tag{16}$$

which gives rise to define the boundary flow and effort variables

$$\begin{bmatrix} \boldsymbol{f}_\partial^t & \boldsymbol{f}_\partial^r & \boldsymbol{e}_\partial^t & \boldsymbol{e}_\partial^r \end{bmatrix}^T = \begin{bmatrix} \boldsymbol{e}^{p_t}|_{\partial Z} & \boldsymbol{e}^{p_r}|_{\partial Z} & \boldsymbol{e}^{\epsilon_t}|_{\partial Z} & \boldsymbol{e}^{\epsilon_r}|_{\partial Z} \end{bmatrix}^T \tag{17}$$

where $\boldsymbol{e}^\nu|_{\partial Z} = \{e^\nu(0), e^\nu(L)\}$, $\nu \in \{p_t, p_r, \epsilon_t, \epsilon_r\}$ denotes the restriction of the effort variables to the boundary of $Z = [0, L]$. Comparing (15) and (16), we get the power continuity equation

$$\int_Z \boldsymbol{e}_b(t,z) \boldsymbol{f}_b(t,z) \, dz + \left(e_\partial^t(t) f_\partial^t(t) + e_\partial^r(t) f_\partial^r(t) \right) \big|_{\partial Z} = 0. \tag{18}$$

The validity (18), is only due to the linear relation $-\boldsymbol{f}_b = (\boldsymbol{P}_1 \partial_z + \boldsymbol{P}_0) \boldsymbol{e}_b$, the application of integration by parts (or Stokes theorem, in general) and the definition of boundary port variables (17). The *(Stokes-)Dirac* structure $\mathcal{D}$ is defined by the corresponding subset of the *bond space* (i. e. the space of conjugated power variables), where power continuity holds. For the subsequent geometric discretization, it is useful to write the distributed part of the (Stokes-)Dirac structure without dissipation[5] as

$$-\boldsymbol{f}_b = \boldsymbol{P}_1 \partial_z \boldsymbol{e}_b + \boldsymbol{P}_0 \boldsymbol{e}_{b*}, \qquad \boldsymbol{e}_{b*} = \boldsymbol{e}_b. \tag{19}$$

We use two different notations for the identical effort vector, depending on whether it is subject to differentiation or not.

[5] The case of dissipation is also discussed in [19].

2.2.2 Structure-preserving spatial discretization

In [19], we performed a geometric or structure-preserving discretization to approximate the infinite-dimensional (Stokes-)Dirac structure by a finite-dimensional counterpart. It is based on the pseudo-spectral method presented in [15] where it has been proposed for canonical systems of two conservation laws. Different polynomial approximation bases are used to take into account the different geometric nature of flow and effort variables. The discretization of the PH system is completed with the finite-dimensional approximation of the energy and the constitutive relations in the approximation spaces. Note that during the whole process the boundary port variables are preserved and appear as (interconnection) port variables (inputs and outputs) in the resulting lumped PH model. The (geometric or structural) properties retained in the lumped model make this method outstanding.

Approximation bases. The idea, see [15], is to define different approximation bases for the flows $f^\nu \in \{f^{p_t},\, f^{p_r},\, f^{\epsilon_t},\, f^{\epsilon_r}\}$ and the efforts $e^\nu \in \{e^{p_t},\, e^{p_r},\, e^{\epsilon_t},\, e^{\epsilon_r}\}$. Different approximation bases are chosen for e^ν and e^ν_*, depending on whether the effort is differentiated or not:

$$f^\nu(t,z) \approx \sum_{k=0}^{N-1} f^\nu_k(t) w^f_k(z), \quad e^\nu_*(t,z) \approx \sum_{k=0}^{N-1} e^\nu_{*,k}(t) w^f_k(z), \qquad e^\nu(t,z) \approx \sum_{i=0}^{N} e^\nu_i(t) w^e_i(z). \tag{20}$$

The time dependent coefficients are collected in the vectors[6]

$$\boldsymbol{f}^\nu, \boldsymbol{e}^\nu_* \in \mathbb{R}^N \quad \text{and} \quad \boldsymbol{e}^\nu \in \mathbb{R}^{N+1}, \qquad \nu \in \{p_t, p_r, \epsilon_t, \epsilon_r\}. \tag{21}$$

$w^f_k(z)$ and $w^e_i(z)$ are the basis functions for flows and efforts that satisfy the exact differentiation or compatibility condition

$$\text{span}\{\partial_z w^e_0, \ldots, \partial_z w^e_N\} \subseteq \text{span}\{w^f_0, \ldots, w^f_{N-1}\} \tag{22}$$

see e. g. [17]. In our problem, the interpolating Lagrange polynomials of degree N and $N-1$ are a suitable choice:

$$w^e_i(z) = \prod_{j=0, j\neq i}^{N} \frac{z-\xi_j}{\xi_i - \xi_j}, \qquad w^f_k(z) = \prod_{j=0, j\neq k}^{N-1} \frac{z-z_k}{z_k - z_j}. \tag{23}$$

$\xi_i \in [0, L]$, $i = 0, \ldots, N$ and $z_k \in [0, L]$, $k = 0, \ldots, N-1$ are the collocation points for w^e_i and w^f_k, respectively, and $w^e_i(\xi_j) = \delta_{ij}$, $w^f_k(z_j) = \delta_{kj}$ hold. The choice of the collocation points will be discussed in detail in Section 3.

Approximation of the structure. Denote $\boldsymbol{w}^e = [w^e_0, \ldots, w^e_N]^T$ the vector of effort basis functions and

$$\boldsymbol{\Phi} = \begin{bmatrix} \boldsymbol{w}^e(0)^T \\ \boldsymbol{w}^e(L)^T \end{bmatrix}. \tag{24}$$

Let $\boldsymbol{f}^{t/r}_\partial = [f^{t/r}_0, f^{t/r}_L]^T$ and $\boldsymbol{e}^{t/r}_\partial = [e^{t/r}_0, e^{t/r}_L]^T$ be the vectors of boundary flows and efforts corresponding to translational and rotational motion. Inserting (20) into (19) and (17), one

[6] Recall that we use the placeholder $\nu \in \{p_t, p_r, \epsilon_t, \epsilon_r\}$.

obtains the linear system of equations

$$
\begin{aligned}
-\begin{bmatrix} \boldsymbol{f}^{p_t} \\ \boldsymbol{f}^{p_r} \\ \boldsymbol{f}^{\epsilon_t} \\ \boldsymbol{f}^{\epsilon_r} \end{bmatrix} &= \begin{bmatrix} \mathbf{0} & \mathbf{0} & \boldsymbol{D} & \mathbf{0} \\ \mathbf{0} & \mathbf{0} & \mathbf{0} & \boldsymbol{D} \\ \boldsymbol{D} & \mathbf{0} & \mathbf{0} & \mathbf{0} \\ \mathbf{0} & \boldsymbol{D} & \mathbf{0} & \mathbf{0} \end{bmatrix} \begin{bmatrix} \boldsymbol{e}^{p_t} \\ \boldsymbol{e}^{p_r} \\ \boldsymbol{e}^{\epsilon_t} \\ \boldsymbol{e}^{\epsilon_r} \end{bmatrix} + \begin{bmatrix} \mathbf{0} & \mathbf{0} & \mathbf{0} & \mathbf{0} \\ \mathbf{0} & \mathbf{0} & \boldsymbol{I}_N & \mathbf{0} \\ \mathbf{0} & -\boldsymbol{I}_N & \mathbf{0} & \mathbf{0} \\ \mathbf{0} & \mathbf{0} & \mathbf{0} & \mathbf{0} \end{bmatrix} \begin{bmatrix} \boldsymbol{e}_*^{p_t} \\ \boldsymbol{e}_*^{p_r} \\ \boldsymbol{e}_*^{\epsilon_t} \\ \boldsymbol{e}_*^{\epsilon_r} \end{bmatrix} \\
\begin{bmatrix} \boldsymbol{f}_\partial^t \\ \boldsymbol{f}_\partial^r \\ \boldsymbol{e}_\partial^t \\ \boldsymbol{e}_\partial^r \end{bmatrix} &= \begin{bmatrix} \boldsymbol{\Phi} & \mathbf{0} & \mathbf{0} & \mathbf{0} \\ \mathbf{0} & \boldsymbol{\Phi} & \mathbf{0} & \mathbf{0} \\ \mathbf{0} & \mathbf{0} & \boldsymbol{\Phi} & \mathbf{0} \\ \mathbf{0} & \mathbf{0} & \mathbf{0} & \boldsymbol{\Phi} \end{bmatrix} \begin{bmatrix} \boldsymbol{e}^{p_t} \\ \boldsymbol{e}^{p_r} \\ \boldsymbol{e}^{\epsilon_t} \\ \boldsymbol{e}^{\epsilon_r} \end{bmatrix}.
\end{aligned}
\tag{25}
$$

The elements of the derivative matrix $\boldsymbol{D} \in \mathbb{R}^{N\times(N+1)}$ are given by the spatial derivative of the effort basis functions at the flow collocation points:

$$
[\boldsymbol{D}]_{k+1,i+1} = \partial_z w_i^e(z_k), \qquad i = 0,\dots,N,\ k = 0,\dots,N-1. \tag{26}
$$

In accordance with the distributed-parameter model, additional couplings through the identity matrices $\boldsymbol{I}_N$ appear on the right hand side of (25).The energy balance (15) is approximated by *degenerate* bilinear forms between the vectors of discrete flows and efforts (for details see [19]):

$$
\dot{H}_b \approx \sum_{\nu\in\{p_t,p_r,\epsilon_t,\epsilon_r\}} (\boldsymbol{e}^\nu)^T \boldsymbol{M} \boldsymbol{f}^\nu. \tag{27}
$$

The elements of the non-square mass matrix $\boldsymbol{M} \in \mathbb{R}^{(N+1)\times N}$ are defined as

$$
[\boldsymbol{M}]_{i,k} = \int_0^L w_i^e(z) w_k^f(z)\, dz.
$$

The subspace of the discrete bond space, on which (25) is defined, is *not* a Dirac structure. The latter requires a *non-degenerate* power pairing, which is obtained by defining vectors of reduced effort variables $\tilde{\boldsymbol{e}}^\nu \in \mathbb{R}^N$,

$$
\tilde{\boldsymbol{e}}^\nu = \boldsymbol{M}^T \boldsymbol{e}^\nu. \tag{28}
$$

Constitutive equations. The energy is approximated by

$$
\bar{H}_b \approx \frac{1}{2} \sum_\nu c^\nu (\boldsymbol{x}^\nu)^T \boldsymbol{S} \boldsymbol{x}^\nu, \quad c^\nu \in \{\frac{1}{\rho}, \frac{1}{I_\rho}, K_s, K_b\}, \tag{29}
$$

where the matrix $\boldsymbol{S} \in \mathbb{R}^{N\times N}$ is made of the elements

$$
[\boldsymbol{S}]_{i,j} = \int_0^L w_i^f(z) w_j^f(z) dz. \tag{30}
$$

On the one hand, we can derive the discretized constitutive

$$
\tilde{\boldsymbol{e}}^\nu = \left(\frac{\partial \bar{H}_b}{\partial \boldsymbol{x}^\nu}\right)^T = c^\nu \boldsymbol{S} \boldsymbol{x}^\nu \quad \forall \nu. \tag{31}
$$

On the other hand, the discretized effort vectors $\boldsymbol{e}_*^\nu$ are defined with respect to the same basis as the states, such that the following relation follows immediately:

$$
\boldsymbol{e}_*^\nu = c^\nu \boldsymbol{x}^\nu = \boldsymbol{S}^{-1} \tilde{\boldsymbol{e}}^\nu = \boldsymbol{S}^{-1} \boldsymbol{M}^T \boldsymbol{e}^\nu. \tag{32}
$$

Input-output representation. The I/O representation, see [19], is derived from elementary matrix operations and assigning the roles of in- and outputs to the boundary port variables. In

$$\begin{bmatrix} \begin{pmatrix} \boldsymbol{f}^{p_t} \\ -e^t_{\partial 0} \end{pmatrix} \\ \begin{pmatrix} \boldsymbol{f}^{p_r} \\ -e^r_{\partial 0} \end{pmatrix} \\ \begin{pmatrix} \boldsymbol{f}^{\epsilon_t} \\ f^t_{\partial L} \end{pmatrix} \\ \begin{pmatrix} \boldsymbol{f}^{\epsilon_r} \\ f^r_{\partial L} \end{pmatrix} \end{bmatrix} = \tilde{\boldsymbol{J}}_b \begin{bmatrix} \begin{pmatrix} \tilde{\boldsymbol{e}}^{p_t} \\ f^t_{\partial 0} \end{pmatrix} \\ \begin{pmatrix} \tilde{\boldsymbol{e}}^{p_r} \\ f^r_{\partial 0} \end{pmatrix} \\ \begin{pmatrix} \tilde{\boldsymbol{e}}^{\epsilon_t} \\ e^t_{\partial L} \end{pmatrix} \\ \begin{pmatrix} \tilde{\boldsymbol{e}}^{\epsilon_r} \\ e^r_{\partial L} \end{pmatrix} \end{bmatrix}, \tag{33}$$

the skew-symmetric (global) interconnection matrix $\tilde{\boldsymbol{J}}_b \in \mathbb{R}^{(4N+4)\times(4N+4)}$ (notation: $\boldsymbol{w}^e_0 = \boldsymbol{w}^e(0)^T$, $\boldsymbol{w}^e_L = \boldsymbol{w}^e(L)^T$) reads

$$\tilde{\boldsymbol{J}}_b = \begin{bmatrix} \boldsymbol{0} & \boldsymbol{0} & \begin{pmatrix} -\boldsymbol{D} \\ -\boldsymbol{w}^e_0 \end{pmatrix} \begin{pmatrix} \boldsymbol{M}^T \\ \boldsymbol{w}^e_L \end{pmatrix}^{-1} & \boldsymbol{0} \\ \boldsymbol{0} & \boldsymbol{0} & \begin{pmatrix} -\boldsymbol{S}^{-1}\boldsymbol{M}^T \\ \boldsymbol{0} \end{pmatrix} \begin{pmatrix} \boldsymbol{M}^T \\ \boldsymbol{w}^e_L \end{pmatrix}^{-1} & \begin{pmatrix} -\boldsymbol{D} \\ -\boldsymbol{w}^e_0 \end{pmatrix} \begin{pmatrix} \boldsymbol{M}^T \\ \boldsymbol{w}^e_L \end{pmatrix}^{-1} \\ \begin{pmatrix} -\boldsymbol{D} \\ -\boldsymbol{w}^e_L \end{pmatrix} \begin{pmatrix} \boldsymbol{M}^T \\ \boldsymbol{w}^e_0 \end{pmatrix}^{-1} & \begin{pmatrix} \boldsymbol{S}^{-1}\boldsymbol{M}^T \\ \boldsymbol{0} \end{pmatrix} \begin{pmatrix} \boldsymbol{M}^T \\ \boldsymbol{w}^e_0 \end{pmatrix}^{-1} & \boldsymbol{0} & \boldsymbol{0} \\ \boldsymbol{0} & \begin{pmatrix} -\boldsymbol{D} \\ -\boldsymbol{w}^e_L \end{pmatrix} \begin{pmatrix} \boldsymbol{M}^T \\ \boldsymbol{w}^e_0 \end{pmatrix}^{-1} & \boldsymbol{0} & \boldsymbol{0} \end{bmatrix}. \tag{34}$$

The following approximate power continuity equation holds:

$$\sum_{\nu\in\{p_t,p_r,\epsilon_t,\epsilon_r\}} (\tilde{\boldsymbol{e}}^\nu)^T \boldsymbol{f}^\nu + \sum_{\mu\in\{t,r\}} (\boldsymbol{e}^\mu_\partial)^T \boldsymbol{f}^\mu_\partial = 0. \tag{35}$$

We denote $\boldsymbol{U}, \boldsymbol{Y} \in \mathbb{R}^4$ the vectors of boundary inputs, and collocated, power-conjugated outputs, which are composed of the elements of the boundary flow and effort vectors f^t_∂, f^r_∂, e^t_∂, e^r_∂, see e. g. [9]. In terms of the physical boundary variables we have

$$\boldsymbol{U}(t) = \begin{bmatrix} \dot{w}(0) \\ \dot{\psi}(0) \\ \hdashline Q_s(L) \\ M_b(L) \end{bmatrix} = \begin{bmatrix} \boldsymbol{U}_0 \\ \boldsymbol{U}_L \end{bmatrix}, \quad \boldsymbol{Y}(t) = \begin{bmatrix} -Q_s(0) \\ -M_b(0) \\ \hdashline \dot{w}(L) \\ \dot{\psi}(L) \end{bmatrix} = \begin{bmatrix} \boldsymbol{Y}_0 \\ \boldsymbol{Y}_L \end{bmatrix}, \tag{36}$$

where $\dot{w}$ and $\dot{\psi}$ denote translational and angular velocity and Q_s and M_b are the shear force and bending moment, respectively. Merging the vectors $\boldsymbol{x}^\nu \in \mathbb{R}^N$ to the overall state vector $\boldsymbol{X} \in \mathbb{R}^{4N}$, we obtain the discretized model in linear PH form:

$$\begin{aligned} \dot{\boldsymbol{X}} &= \boldsymbol{J}_b \left(\frac{\partial \bar{H}_b}{\partial \boldsymbol{X}} \right)^T + \boldsymbol{B}_b \boldsymbol{U} \\ \boldsymbol{Y} &= \boldsymbol{B}_b^T \left(\frac{\partial \bar{H}_b}{\partial \boldsymbol{X}} \right)^T + \boldsymbol{D}_b \boldsymbol{U} \end{aligned} \tag{37}$$

where $\boldsymbol{J}_b$, $\boldsymbol{B}_b$ and $\boldsymbol{D}_b$ are composed of the corresponding submatrices of $\tilde{\boldsymbol{J}}$. In particular, we write the input and feedthrough[7] matrices

$$\boldsymbol{B}_b = \begin{bmatrix} \boldsymbol{B}_0 & \boldsymbol{B}_L \end{bmatrix}, \qquad \boldsymbol{D}_b = \begin{bmatrix} \boldsymbol{D}_0 & \boldsymbol{D}_I \\ -\boldsymbol{D}_I^T & \boldsymbol{D}_L \end{bmatrix}, \ \boldsymbol{D}_0 = -\boldsymbol{D}_0^T, \ \boldsymbol{D}_L = -\boldsymbol{D}_L^T. \tag{38}$$

[7] The feedthrough stems from the rigid body motion.

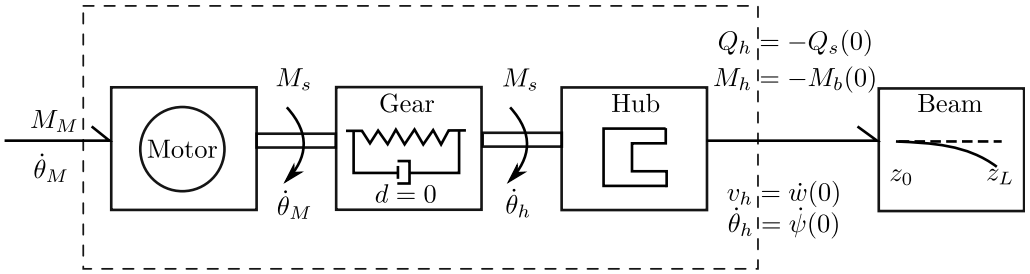

Figure 4: Symbolic representation of the interconnected system. The half arrows indicate the direction of the power flow.

2.3 Coupling of the subsystems

The flexible beam is attached to the rigid hub. The point $z = 0$ along the beam corresponds to the radius of the hub. Here, the (reaction) shear force is localized. The power-preserving interconnection conditions, which are visualized in Fig. 4, are

$$\begin{aligned} \boldsymbol{u}_{a_2} &= \begin{bmatrix} -Q_h & -M_h \end{bmatrix}^T = -\boldsymbol{Y}_0 = \begin{bmatrix} Q_s(0) & M_b(0) \end{bmatrix}^T, \\ \boldsymbol{y}_{a_2} &= \begin{bmatrix} v_h & \dot{\theta}_h \end{bmatrix}^T \quad\quad = \boldsymbol{U}_0 = \begin{bmatrix} \dot{w}(0) & \dot{\psi}(0) \end{bmatrix}^T. \end{aligned} \tag{39}$$

Inserting the corresponding parts of (33) and (8) into (39), we obtain

$$\begin{aligned} \boldsymbol{u}_{a_2} &= -\boldsymbol{Y}_0 = -\left(\boldsymbol{B}_0^T \left(\frac{\partial \bar{H}_b}{\partial \boldsymbol{X}} \right)^T + \boldsymbol{D}_I \boldsymbol{U}_L \right), \\ \boldsymbol{U}_0 &= \boldsymbol{Y}_{a_2} = \boldsymbol{B}_{a_2}^T \left(\frac{\partial H_a}{\partial \boldsymbol{x}_a} \right)^T. \end{aligned} \tag{40}$$

We can rewrite the differential equations for the drive system and the discretized beam as

$$\begin{aligned} \dot{\boldsymbol{x}}_a &= \boldsymbol{J}_a \left(\frac{\partial H_a}{\partial \boldsymbol{x}_a} \right)^T - \boldsymbol{B}_{a_2} \boldsymbol{B}_0^T \left(\frac{\partial \bar{H}_b}{\partial \boldsymbol{X}} \right)^T + \boldsymbol{B}_{a_1} u_{a_1} - \boldsymbol{B}_{a_2} \boldsymbol{D}_I \boldsymbol{U}_L \\ \dot{\boldsymbol{X}} &= \boldsymbol{B}_0 \boldsymbol{B}_{a_2}^T \left(\frac{\partial H_a}{\partial \boldsymbol{x}_a} \right)^T + \boldsymbol{J}_b \left(\frac{\partial \bar{H}_b}{\partial \boldsymbol{X}} \right)^T + \boldsymbol{B}_L \boldsymbol{U}_L, \end{aligned} \tag{41}$$

With the global state vector $\tilde{\boldsymbol{x}} = [\boldsymbol{x}_a^T, \boldsymbol{X}^T]^T \in \mathbb{R}^{4N+4}$, the total energy $\tilde{H}(\tilde{\boldsymbol{x}}) = H_a(\boldsymbol{x}_a) + \overline{H}_b(\boldsymbol{X})$ and the definition of the global inputs and their collocated, power-conjugated outputs

$$\tilde{\boldsymbol{u}} = \begin{bmatrix} u_{a_1} \\ \boldsymbol{U}_L \end{bmatrix} = \begin{bmatrix} M_M \\ \bar{Q}_s(\bar{L}) \\ M_b(L) \end{bmatrix}, \qquad \tilde{\boldsymbol{y}} = \begin{bmatrix} y_{a_1} \\ \boldsymbol{Y}_L \end{bmatrix} = \begin{bmatrix} \dot{\theta}_M \\ \bar{\dot{w}}(\bar{L}) \\ \dot{\psi}(L) \end{bmatrix}, \tag{42}$$

we obtain the state space model in standard PH form

$$\begin{aligned} \dot{\tilde{\boldsymbol{x}}} &= \begin{bmatrix} \boldsymbol{J}_a & -\boldsymbol{B}_{a_2} \boldsymbol{B}_0^T \\ \boldsymbol{B}_0 \boldsymbol{B}_{a_2}^T & \boldsymbol{J}_b \end{bmatrix} \left(\frac{\partial \tilde{H}}{\partial \tilde{\boldsymbol{x}}} \right)^T + \begin{bmatrix} \boldsymbol{B}_{a_1} & -\boldsymbol{B}_{a_2} \boldsymbol{D}_I \\ \boldsymbol{0} & \boldsymbol{B}_L \end{bmatrix} \tilde{\boldsymbol{u}} \\ \tilde{\boldsymbol{y}} &= \begin{bmatrix} \boldsymbol{B}_{a_1}^T & \boldsymbol{0} \\ -\boldsymbol{D}_I^T \boldsymbol{B}_{a_2}^T & \boldsymbol{B}_L \end{bmatrix} \left(\frac{\partial \tilde{H}}{\partial \tilde{\boldsymbol{x}}} \right)^T. \end{aligned} \tag{43}$$

By skew-symmetry of the overall structure matrix and the relation between input and power-conjugated output, we obtain immediately the overall energy balance

$$\dot{\tilde{H}} = \dot{H}_a + \dot{\tilde{H}}_b = \boldsymbol{y}_a^T \boldsymbol{u}_a + \boldsymbol{Y}^T \boldsymbol{U} = \tilde{\boldsymbol{y}}^T \tilde{\boldsymbol{u}}. \tag{44}$$

Without a tip mass, $\boldsymbol{U}_L = \begin{bmatrix} Q_s(L) & M_b(L) \end{bmatrix}^T = \boldsymbol{0}$, i. e. the interconnected model of the flexible set-up is only driven by the motor torque.

3 Comments on the geometric pseudo-spectral discretization

In this section, we discuss in detail some issues that are related to the application of the geometric pseudo-spectral method and its approximation quality for the flexible beam example. We discuss the approximation of the spectrum and the eigenfunctions under homogeneous boundary conditions and the approximation of a transfer function for a time-varying boundary condition.

3.1 Choice of the collocation points for the basis functions

A core ingredient of the geometric pseudo-spectral method is the choice of the approximation space. In section 2.2.2, interpolating Lagrange polynomials, which satisfy the compatibility condition (22), are chosen as basis functions. The collocation points, where the approximate solution should match the exact one, can be typically either uniformly distributed or chosen as the zeros of Legendre or Chebyshev polynomials. Since the boundary flows and efforts depend on the boundary conditions, the two endpoints are also taken into account (see [10]).
Let us consider the clamped-free boundary conditions ($\theta_h(t) = 0$, free tip) for which the exact solution can be calculated by separation of variables (see Appendix A.2) with computer algebra software like Maple®. The four boundary conditions in terms of boundary flows/efforts are:

$$\begin{array}{lll} \text{Clamped at } z = 0\text{:} & \dot{w}(t,0) = 0, & \dot{\psi}(t,0) = 0. \\ \text{Free at } z = L\text{:} & Q_s(t,L) = 0, & M_b(t,L) = 0. \end{array} \tag{45}$$

We consider different distributions of collocation points: uniformly distributed and in the zeros of Gauss-Legendre polynomials plus the two endpoints of the interval. Table 2 shows the natural frequencies for the discretized system with different N, compared to the exact values according to Appendix A.2. The method is *conservative*, i. e. no numerical dissipation occurs in the approximate models. It is remarkable that the approximate eigenfrequencies do not depend on the choice of the collocation points[8]. Note that the first five eigenfrequencies – which are dominant for control – are very well approximated even with a relatively small number of collocation points (here $N = 12$).
Contrary to the eigenfrequencies, the distribution of collocation points has a strong impact on the approximation of the eigenfunctions. To avoid the occurrence of numerical oscillations at the boundaries of the interval $[0, L]$ with increasing number N of collocation points (*Runge's phenomenon*, see e. g. [7]), we choose the interior Gauss-Legendre collocation points together with the two endpoints in this contribution.

3.2 Approximation of the eigenfunctions

We compare the eigenfunctions based on the single fourth order displacement differential equation as derived in Appendix A with the numerical approximations by the geometric pseudo-spectral

[8] See also the discussion of this point in [15], p. 1290.

Table 2: First five natural frequencies of the discretized model for the uniform beam in Hz.

Exact frequency	Uniformly distributed		Gauss-Legendre	
	$N = 6$	$N = 12$	$N = 6$	$N = 12$
9.8873	9.8873	9.8873	9.8873	9.8873
61.9447	61.9463	61.9447	61.9463	61.9447
173.3663	174.294	173.3663	174.2940	173.3663
339.4978	371.4142	339.4978	371.4142	339.4978
560.7196	964.2529	560.7327	964.2529	560.7327

method. Under homogeneous boundary conditions, it is easy to obtain the exact eigenfunctions (eigenmodes) for the corresponding eigenfrequencies. The approximate eigenfunctions can be represented as the weighted sum of corresponding flow/state basis functions

$$\hat{X}_i(z) = \sum_{k=0}^{N-1} X_i(z_k) w_k^f(z) \tag{46}$$

with $X_i(z_k)$ the exact values of the i-th eigenfunction in the collocation points z_k (see also [17]). Figure 5 represents the approximations of the first (left) and fifth (right) eigenfunctions, compared to the exact eigenfunctions. The first eigenfunction is perfectly approximated with $N = 6$, while for the fifth one, $N = 12$ is large enough to achieve "perfect" matching.

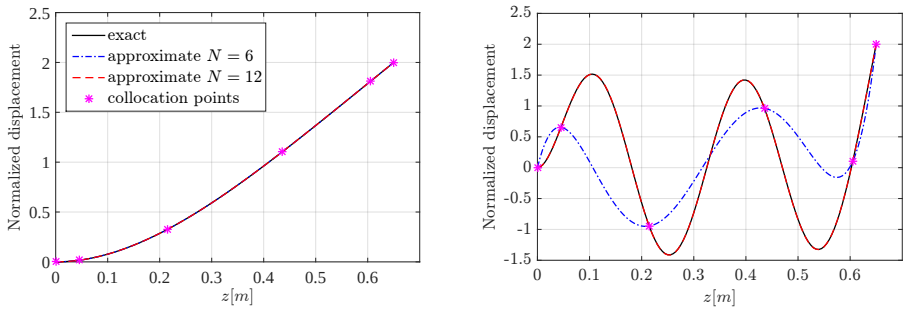

(a) First eigenfunction. (b) Fifth eigenfunction.

Figure 5: Exact and approximate eigenfunctions for the first and fifth mode.

3.3 Approximation of the transfer function

Neglecting the drive system, we consider the forced rotation of the beam around the joint at $z = 0$, which means that the second boundary condition in (45) becomes time-varying: $\dot{\psi}(t, 0) = \dot{\theta}_h(t)$. The exact transfer function between $\dot{\psi}(t, 0)$ and $\dot{\psi}(t, L)$, is evaluated numerically (see Appendix A.3). In Fig. 6, this exact amplitude frequency response (solid line) is compared with the transfer functions of the discretized models with $N = 6$ (dash-dotted) and $N = 12$ (dashed). The latter approximation fits perfectly the exact frequency response in the considered range.
To sum up this section, the geometric discretization approach using interpolating Lagrange polynomials gives an accurate approximation of eigenfrequencies, eigenfunctions and the transfer behavior, even for small N.

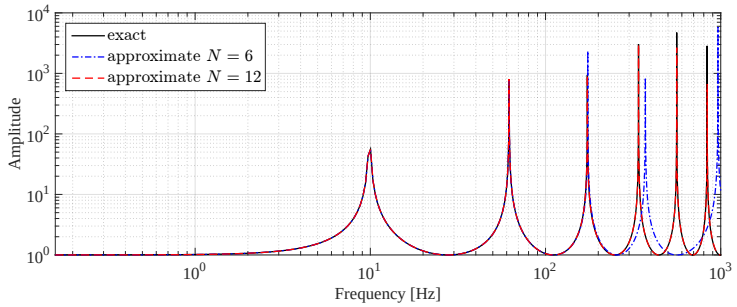

Figure 6: Exact and approximate amplitude frequency response from $\dot{\psi}(t, 0)$ to $\dot{\psi}(t, L)$.

4 Conclusions and outlook

We presented the modeling of a single-link light-weight manipulator in the port-Hamiltonian (PH) framework by interconnecting the drive system with gear elasticity and the flexible link. The finite-dimensional model for the Timoshenko beam has been obtained using a geometric pseudo-spectral method in PH formulation. We discussed in some detail the choice of the collocation points and the approximation accuracy of the beam model in terms of spectrum, eigenfunctions and the frequency response.
The structure of the PH beam model can be exploited for inversion-based feedforward motion control [19]. Current work is on implementing the feedforward controller – including the model of the flexible drive – on the test rig and performing first experiments. In a next step, to achieve highly dynamic motion control, we will close the loop by observer-based feedback control in the PH framework [8]. The single flexible-link setup is the simplest configuration of the modular flexible test rig. The extension to a multibody flexible-link manipulator, and its operation based on PH models poses a series of interesting research questions in theory and application.

References

[1] J. Damerau. *Untersuchung der dynamischen Eigenschaften von Balken mit fraktionalen Stoffgesetzen*. PhD thesis, Helmut Schmidt University, Hamburg, 2008.

[2] V. Duindam, A. Macchelli, S. Stramigioli, and H. Bruyninckx. *Modeling and control of complex physical systems: the port-Hamiltonian approach*. Springer Science & Business Media, 2009.

[3] Y. Q. Gao, F. Y. Wang, and Z. Q. Xiao. *Flexible Manipulators: Modeling, Analysis and Optimum Design*. Academic Press, 2012.

[4] H. Gattringer. *Starr-elastische Robotersysteme: Theorie und Anwendungen*. Springer-Verlag, 2011.

[5] H. Gattringer and J. Gerstmayr. *Multibody system dynamics, robotics and control*. Springer Science & Business Media, 2013.

[6] G. Golo, V. Talasila, A. van der Schaft, and B. Maschke. *Hamiltonian discretization of boundary control systems*. Automatica, 40(5):757–771, May 2004.

[7] J. S. Hesthaven. *From electrostatics to almost optimal nodal sets for polynomial interpolation in a simplex*. SIAM Journal on Numerical Analysis, 35(2):655–676, 1998.

[8] P. Kotyczka and M. Wang. *Dual observer-based compensator design for linear port-Hamiltonian systems*. In Control Conference (ECC), 2015 European, pages 2908–2913. IEEE, 2015.

[9] Y. Le Gorrec, H. Zwart, and B. Maschke. *Dirac structures and boundary control systems associated with skew-symmetric differential operators*. SIAM Journal on Control and Optimization, 44(5):1864–1892, 2005.

[10] J. Lee and W. Schultz. *Eigenvalue analysis of Timoshenko beams and axisymmetric Mindlin plates by the pseudospectral method*. Journal of Sound and Vibration, 269(3):609–621, 2004.

[11] M. Loudini, D. Boukhetala, M. Tadjine, and M. Boumehdi. *Application of Timoshenko beam theory for deriving motion equations of a lightweight elastic link robot manipulator*. CGST-ARAS Journal, 5:11–18, 2006.

[12] A. Macchelli. *Energy shaping of distributed parameter port-Hamiltonian systems based on finite element approximation*. Syst. Control Lett., 60:579–589, 2011.

[13] A. Macchelli, C. Melchiorri, and S. Stramigioli. *Port-based modeling and simulation of mechanical systems with rigid and flexible links*. IEEE Transactions on Robotics, 25(5):1016–1029, 2009.

[14] L. Majkut. *Free and forced vibrations of Timoshenko beams described by single difference equation*. Journal of Theoretical and Applied Mechanics, 47(1):193–210, 2009.

[15] R. Moulla, L. Lefèvre, and B. M. Maschke. *Pseudo-spectral methods for the spatial symplectic reduction of open systems of conservation laws*. Journal of Computational Physics, 231(4):1272–1292, 2012.

[16] A. Siuka, M. Schöberl, and K. Schlacher. *Port-Hamiltonian modelling and energy-based control of the Timoshenko beam*. Acta mechanica, 222(1-2):69–89, 2011.

[17] N. M. T. Vu, L. Lefèvre, R. Nouailletas, and S. Brémond. *Geometric discretization for a plasma control model*. IFAC Proceedings Volumes, 46(2):755–760, 2013.

[18] D. Wang and M. Vidyasagar. *Transfer functions for a single flexible link*. The International journal of robotics research, 10(5):540–549, 1991.

[19] M. Wang, A. Bestler, and P. Kotyczka. *Modeling, discretization and motion control of a flexible beam in the port-Hamiltonian framework*. In 20th IFAC World Congress, 2017.

Appendix A Free and forced vibrations of the Timoshenko beam

We sketch the derivation of exact expressions for the eigenforms and the computation of the natural frequencies of the Timoshenko beem as described in [14]. Moreover, we summarize the reasoning of [1] to obtain transfer functions for the case of inhomogeneous boundary conditions.

A.1 Eigenvalue problem

Setting $w(t,z) = T(t)X(z)$ and $\psi(t,z) = T(t)Y(z)$, the two PDEs (9) can be written

$$\begin{aligned} \rho X(z)\ddot{T}(t) - K_s[X^{''}(z)T(t) - Y^{'}(z)T(t)] = 0, \\ I_\rho Y(z)\ddot{T}(t) + K_s[Y(z)T(t) - X^{'}(z)T(t)] - K_b Y^{''}T(t) = 0. \end{aligned} \tag{47}$$

Separation of variables yields

$$\frac{\ddot{T}}{T} = \frac{K_s(X'' - Y')}{\rho X} = \frac{K_b Y'' - K_s(Y - X')}{I_\rho Y}. \tag{48}$$

For harmonic vibrations with frequency ω, the time function satisfies $\ddot{T}(t) + \omega^2 T(t) = 0$. Using this relation, we arrive quickly at the expressions

$$Y' = X'' + a(\omega)X \tag{49}$$

$$-b(\omega)Y = X''' + [a(\omega) + c(\omega)]X' \tag{50}$$

with the frequency-dependent coefficients

$$a(\omega) = \frac{\rho\omega^2}{K_s}, \quad b(\omega) = \frac{I_\rho\omega^2}{K_b} - \frac{K_s}{K_b}, \quad c(\omega) = \frac{K_s}{K_b}. \tag{51}$$

From (49), (50), we eliminate Y to obtain the single fourth order differential equation for the displacement function

$$X^{(4)} + d(\omega)X^{''} + e(\omega)X = 0, \tag{52}$$

where[9]

$$d(\omega) = a(\omega) + b(\omega) + c(\omega) = \omega^2(\frac{I_\rho}{K_b} + \frac{\rho}{K_s}), \qquad e(\omega) = a(\omega)b(\omega) = \frac{\rho\omega^2}{K_b}(\frac{I_\rho\omega^2}{K_s} - 1). \tag{53}$$

By parametrizing the solutions of (52) via $X(z) = Ce^{\lambda z}$, we obtain the characteristic equation

$$\lambda^{(4)} + d(\omega)\lambda^2 + e(\omega) = 0. \tag{54}$$

With $r := \lambda^2$, this becomes a quadratic equation whose roots are given by

$$r_{1/2} = -\frac{1}{2}d(\omega) \pm \frac{1}{2}\sqrt{\Delta(\omega)}, \qquad \Delta(\omega) = d^2(\omega) - 4e(\omega) > 0 \quad \forall\omega. \tag{55}$$

At the critical frequency $\omega_c = \sqrt{\frac{\kappa GA}{I\rho_v}}$, the root r_1 changes sign, while $r_2 < 0$ for all ω. We distinguish the cases

1. $\omega < \omega_c \;\Rightarrow\; r_1 > 0$. The resulting pairs of real and complex eigenvalues are

$$\pm\lambda_1 = \pm\sqrt{r_1}, \quad \pm i\lambda_2 = \pm i\sqrt{-r_2}. \tag{56}$$

[9]The coefficients in terms of the volume density $\rho_v = \frac{\rho}{A}$ and the moment of inertia $I = \frac{I_\rho}{\rho_v}$ read

$$a = \frac{\rho_v\omega^2}{\kappa G}, \quad b = \frac{\rho_v\omega^2}{E} - c(\omega), \quad c = \frac{\kappa GA}{EI}, \quad d = \omega^2\rho_v(\frac{1}{E} + \frac{1}{\kappa G}), \quad e = \frac{\omega^2}{EI}(\frac{I\rho_v^2\omega^2}{\kappa G} - A\rho_v).$$

2. $\omega > \omega_c \;\Rightarrow\; r_1 < 0$. Only pairs of complex eigenvalues occur:

$$\pm i\lambda_1 = \pm i\sqrt{-r_1}, \quad \pm i\lambda_2 = \pm i\sqrt{-r_2}. \tag{57}$$

We consider only the first case and describe the eigenvalues and eigenforms for the (dominant) lower frequencies. The general solution of the displacement function $X(z)$ be written as

$$\begin{aligned} X(z) &= C_1 e^{\lambda_1 z} + C_2 e^{-\lambda_1 z} + C_3 e^{i\lambda_2 z} + C_4 e^{-i\lambda_2 z} \\ &= P_1 \cosh(\lambda_1 z) + P_2 \sinh(\lambda_1 z) + P_3 \cos(\lambda_2 z) + P_4 \sin(\lambda_2 z) \end{aligned} \tag{58}$$

with $P_{1/2} = C_1 \pm C_2$ and $P_{3/4} = C_3 \pm C_4$.

A.2 Boundary conditions, eigenforms and natural frequencies

The clamped-free boundary conditions with $\theta_h = 0$ are translated into conditions on $X(z)$:

$$\begin{aligned} X(0) &= 0, & X'''(0) + (a(\omega) + c(\omega))X'(0) &= 0, \\ X'''(L) + dX'(L) &= 0, & X''(L) + aX(L) &= 0. \end{aligned} \tag{59}$$

With the general solution (58) for $X(z)$ and its derivatives, we can formulate a system of equations for the free parameters that satisfy the boundary conditions (abbreviations: $A = \cosh(\lambda_1 L)$, $B = \sinh(\lambda_1 L)$, $C = \cos(\lambda_2 L)$, $D = \sin(\lambda_2 L)$):

$$\begin{bmatrix} 1 & 0 & 1 & 0 \\ 0 & \lambda_1((a+c) + \lambda_1^2) & 0 & \lambda_2((a+c) - \lambda_2^2) \\ \lambda_1(\lambda_1^2 + d)B & \lambda_1(\lambda_1^2 + d)A & \lambda_2(\lambda_2^2 - d)D & -\lambda_2(\lambda_2^2 - d)C \\ (\lambda_1^2 + a)A & (\lambda_1^2 + a)B & (-\lambda_2^2 + a)C & (-\lambda_2^2 + a)D \end{bmatrix} \begin{bmatrix} P_1 \\ P_2 \\ P_3 \\ P_4 \end{bmatrix} = \begin{bmatrix} 0 \\ 0 \\ 0 \\ 0 \end{bmatrix}. \tag{60}$$

This system of equations has the form

$$\boldsymbol{M}(\omega)\boldsymbol{P} = \boldsymbol{0} \tag{61}$$

with a matrix $\boldsymbol{M}(\omega)$, whose entries depend on the frequency ω, and $\boldsymbol{P} = \begin{bmatrix} P_1 & P_2 & P_3 & P_4 \end{bmatrix}^T$. The frequencies at which $\det \boldsymbol{M}(\omega) = 0$, are the *natural frequencies* or eigenfrequencies ω_i of the cantilever beam. The corresponding non-zero values of $\boldsymbol{P}$ parametrize the associated eigenfunctions/eigenforms $X_i(z)$ of the free vibration[10].

A.3 Inhomogeneous boundary conditions

To obtain a transfer function from the hub angular velocity to the rotation speed of the tip, we assume a harmonic excitation $\theta_h(\omega)$ of the hub angle. The second boundary condition in (59) is in this case replaced by

$$-b(\omega)\theta_h(\omega) = X''' + (a(\omega) + c(\omega))X'. \tag{62}$$

[10]The eigenfunctions can be normalized by requiring (see e. g. [18])

$$\langle X_i(z), X_j(z) \rangle = \begin{cases} \delta_{ij}, & i = j \\ 0, & i \neq j \end{cases}, \qquad \forall i, j.$$

The system of equations (61) becomes inhomogeneous,

$$\boldsymbol{M}(\omega)\boldsymbol{P} = \boldsymbol{K}(\omega), \tag{63}$$

with $\boldsymbol{K}(\omega) = \begin{bmatrix} 0 & -b(\omega)\theta_h(\omega) & 0 & 0 \end{bmatrix}^T$. For $\det \boldsymbol{M}(\omega) \neq 0$, we can express the coefficients of the general solution as $\boldsymbol{P} = \boldsymbol{M}^{-1}(\omega)\boldsymbol{K}(\omega)$, which allows us to establish the relation

$$Y(\omega, L) = G(\omega)\theta_h(\omega). \tag{64}$$

between the hub angle and the rotation of the beam tip. The same transfer function $G(\omega)$ describes the ratio between the angular velocities.